The Astronomical Journal, 133:2487–2494, 2007 June

VERA 22 GHz FRINGE SEARCH SURVEY

Leonid Petrov[1]
Mizusawa Astrogeodynamics Observatory, NAOJ, Mizusawa 023-0861, Japan; leonid.petrov@lpetrov.net

Tomoya Hirota
National Astronomical Observatory of Japan, Mitaka 181-8588, Tokyo, Japan; tomoya.hirota@nao.ac.jp

Mareki Honma and Katsunori M. Shibata
Mizusawa VERA Observatory, NAOJ, Mitaka 181-8588, Tokyo, Japan;
honmamr@cc.nao.ac.jp, k.m.shibata@nao.ac.jp

and

Takaaki Jike and Hideyuki Kobayashi
Mizusawa Astrogeodynamics Observatory, NAOJ, Mizusawa 023-0861, Japan;
jike@miz.nao.ac.jp, hideyuki.kobayashi@nao.ac.jp
Received 2006 September 19; accepted 2007 January 24

ABSTRACT

This paper presents results of a survey search for bright compact radio sources at 22 GHz with the VERA radio interferometer. Each source from a list of 2494 objects was observed in one scan for 2 minutes. The purpose of this survey was to find compact extragalactic sources bright enough at 22 GHz to be useful as phase calibrators. Observed sources were either (1) within 6° of the Galactic plane, or (2) within 11° of the Galactic center, or (3) within 2° of known water masers. Among the observed sources, 549 were detected, including 180 extragalactic objects that were not previously observed with the very long baseline interferometry technique. Estimates of the correlated flux densities of the detected sources are presented. It was found that the probability of detecting a 200 mJy source with 120 s of integration time is 60%.

Key words: catalogs — radio continuum: general — surveys

Online material: machine-readable tables

1. INTRODUCTION

The VLBI Exploration of Radio Astrometry (VERA) is a Japanese VLBI array dedicated to phase-referencing astrometry to explore the Milky Way (Honma et al. 2000a; Kobayashi et al. 2004). VERA observes Galactic H_2O and SiO maser sources and determines their parallax and proper motions at the 10 μas accuracy level. Based on the high-precision astrometry of $\sim$1000 maser sources, VERA will study the three-dimensional structure and dynamics of the Galaxy's disk and bulge, revealing the true shape of the bulge and spiral arms, its precise rotation curve, and the distribution of dark matter.

The VERA array consists of four 20 m diameter radio telescopes spread over Japan, covering baselines ranging from 1000 to 2300 km (Fig. 1). Unlike other VLBI stations, VERA telescopes are equipped with a dual-beam system (Kawaguchi et al. 2000), with which one can simultaneously observe two sources separated from each other by up to 100 times the telescope's primary beam size. With such a system, VERA can observe a Galactic maser source and an extragalactic calibrator source at the same time and perform relative astrometry of the Galactic maser source with respect to the extragalactic calibrator, which serves as a position reference. Simultaneous observations of two sources, rather than switching observations with single-beam telescopes, are expected to be more effective in canceling out the tropospheric fluctuations, which are the main source of position error in differential VLBI astrometry at 22 GHz or higher frequency. In fact, preliminary results from VERA's dual-beam system observations have already shown its high capability of phase referencing to reach down to 10 μas level accuracy (Honma et al. 2003), and now monitoring of several bright maser sources is ongoing to produce initial results from the VERA.

In order to observe a pair of two adjacent sources with VERA, the separation angle of the pair must be less than 2.2°. This is not only a mechanical limit of VERA's dual-beam system, but also a practical limit for effective phase referencing to achieve 10 μas accuracy; i.e., the reference source needs to be close enough to the target maser to remove the tropospheric fluctuations sufficiently. Therefore, the existence of calibrators close to target sources is crucial to successful VERA observations. If we assume a uniform density of calibrators in the sky plane, $\sim$2700 calibrators are required in the whole sky to find a calibrator within 2.2° of any sky position (a circle with radius of 2.2° covers 0.0046 sr in the sky; thus, $4\pi/0.0046 \approx 2700$ is necessary). Practically, however, more sources are needed because the distribution over the sky is not uniform.

To date, there have been many efforts to find good calibrators observable with VLBI. A source is considered as a good calibrator if it is compact and bright enough to be detected at the longest baselines for a time less than the coherence limit set by the propagation media. The pioneering work of Cohen & Shaffer (1971) provided the first catalog of source positions determined with VLBI, which contained 35 strong sources. In 1998 the International Celestial Reference Frame (ICRF) catalog of 667 sources produced by analyzing VLBI observations made in the framework of space geodesy programs was published by Ma et al. (1998). At present, the most massive survey of compact calibrators is the VLBA Calibrator Survey (VCS), performed in 1994–2005

[1] On leave from NVI, Inc./NASA Goddard Space Flight Center.

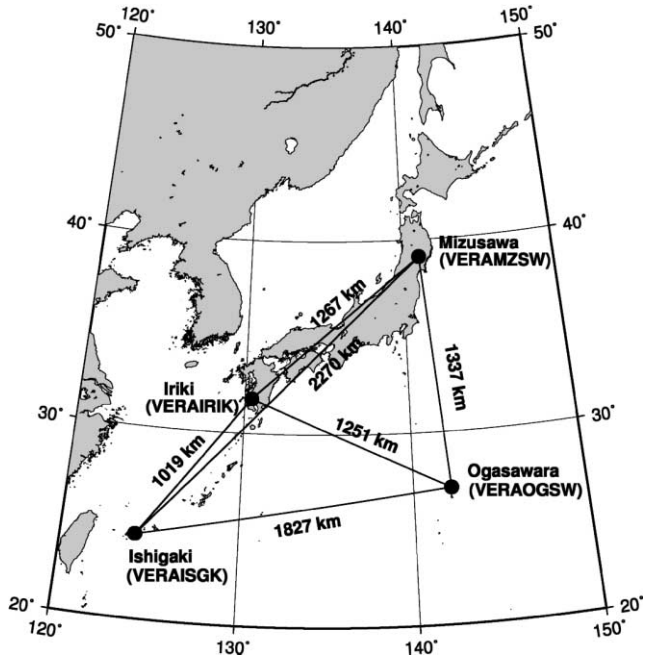

FIG. 1.—VERA network.

(Beasley et al. 2002; Fomalont et al. 2003; Petrov et al. 2005, 2006; Kovalev et al. 2007). After the fifth VCS campaign, the NASA catalog 2005f_astro[2] of all sources detected in the absolute astrometry mode at 2.2 and/or 8.6 GHz frequency bands (S and X) contains 3481 sources. Among them, 85% are acceptable as calibrators for the VLBA. Nevertheless, in the sky area at $\delta \geq -40^\circ$, which is observable with VERA, the probability of finding an X/S calibrator with correlated flux density over 60 mJy within 2.2° of any position is ~70% (Petrov et al. 2006), indicating that more calibrators are needed in order to observe all maser sources with VERA. Moreover, maser sources tend to be confined to the Galactic plane, because they are basically located in the Galaxy's disk, but the density of known calibrators near the Galactic plane is even lower than that in other sky regions. This is due to the strategies used to find compact calibrators: the list of candidates was based on low-resolution sky surveys that severely suffered from strong radio foreground in the Galactic plane. Besides, some past surveys, e.g., the Jodrell Bank—VLA Astrometric Survey (JVAS; Wrobel et al. 1998), VCS1, VCS3, and VCS4, specifically avoided the Galactic plane. To overcome this problem, a calibrator survey in the Galactic plane has been performed by Honma et al. (2000b), finding more than 50 new calibrators at $|b| \leq 5^\circ$, but many more calibrators in this region are still needed.

For these reasons, we have been performing the Galactic Plane Survey (GaPS) of compact radio sources, based on the VERA and VLBA observations. The objective of this campaign is to provide a list of calibrators for dual-beam VERA observations of H_2O masers at 22 GHz. It is much harder to find a good calibrator at 22 GHz and high frequencies, since in general sources are weaker at high frequencies, and the tropospheric fluctuations set a rather short limit to the integration time. Our strategy for GaPS is twofold: first, we observe a wide list of candidate sources with VERA, and then observe a narrow list of detected sources with the VLBA in order to determine their positions at the 1–10 nrad level of accuracy and to obtain high-quality maps. In this paper we present results from the first part of the GaPS project, the fringe search observations with the VERA, reporting the detection of 180 new compact sources. In § 2 we describe our approach to the selection of candidates, scheduling, and observations. In § 3 we describe our analysis of the observations. Results are discussed in § 4, and concluding remarks are given in § 5.

2. OBSERVATIONS

2.1. *Source Selection*

We searched for compact extragalactic sources with correlated flux density >100 mJy at spacings of $\sim 10^8$ wavelengths at 22 GHz in the following zones: (1) $|b| < 6^\circ$ and $\delta > -40^\circ$; (2) within an 11° radius of the Galactic center; and (3) within 2.2° of objects listed in the second update of the Arcetri Catalog of H_2O maser sources (Valdettaro et al. 2001) and the stellar masers catalog of Benson et al. (1990).

First, we combed through the wide list of 3481 known compact sources observed and detected under absolute astrometry programs at S/X bands by 2005 December. Among them, 510 fall in our zones of interest. Also among the 3481 known compact sources, 252 objects have been observed under the K/Q band survey in 2002–2005 (Fey et al. 2005; Jacobs et al. 2005), and can be considered as confirmed K-band calibrators. But only 16 of these fall in our zones of interest. The first list of targets was formed from the 510 known X-band calibrators, except 16 objects observed with the K/Q band survey. The purpose of including known X/S calibrators in the list of candidate sources was to check whether they are bright enough at K band to be detected. It was expected that not all of these would be detected with VERA, since although they have correlated flux densities above 60 mJy at X band, their correlated flux densities at K band may be below the VERA detection limit and, therefore, not suitable as calibrators for VERA.

Second, we searched the CATS database (Verkhodanov et al. 1997) containing almost all radio catalogs[3] to find flux density measurements at radio frequencies 1.4 MHz and higher. We selected the sources with at least two measurements of the flux density and found their spectral index by fitting a straight line to the $\log F / \log f$ dependence, where F is the flux density and f is the frequency. The flux density was extrapolated to 22 GHz. Those sources in the zone of our interest, which had extrapolated flux density >100 mJy at 22 GHz, and which were not observed in the absolute astrometry mode, were put in the second list of targets, in total 1901 new sources.

2.2. *Scheduling*

The list of target sources was split into two groups: the first group was of 1386 objects within 6° of the Galactic plane or within 11° of the Galactic center, and the second group was of 1032 sources within 2.2° of known Galactic maser sources. The first group had priority in scheduling. Among target sources, 94% were observed in one scan of 120 s, and 6% were observed in two scans. Observing schedules were prepared using the following procedure. A source in the target list, which was not observed in previous experiments and which had the highest elevation at the station of VERZMZSW, was selected as the

[2] Available at http://vlbi.gsfc.nasa.gov/astro.

[3] See http://cats.sao.ru/doc/CATS_list.html.

TABLE 1
Observing Sessions

Session Name	Start Date	Duration (hr)	No. Stations	Accumulation Period Length (s)
r05284b.....	2005 Oct 11 08:20	7.0	3	1.0
r05285b.....	2005 Oct 12 08:20	7.0	4	1.0
r05332b,c	2005 Nov 28 12:20	10.8	4	1.0
r05335b.....	2005 Dec 1 11:00	12.5	4	1.0
r05343b.....	2005 Dec 9 15:00	8.5	4	0.1
r05348a.....	2005 Dec 14 09:00	14.0	3	1.0
r05349a.....	2005 Dec 15 10:00	20.0	3	1.0
r05350a.....	2005 Dec 16 07:00	7.5	3	1.0
r05350b.....	2005 Dec 16 14:55	8.5	3	1.0
r05353d.....	2005 Dec 19 04:00	5.5	3	1.0
r05359d.....	2005 Dec 25 02:00	7.0	4	0.1
r06052b.....	2006 Feb 21 18:00	13.0	4	0.1
r06054a.....	2006 Feb 23 19:00	11.0	4	0.1
r06059b.....	2006 Feb 28 18:00	16.0	4	0.1

first object in the schedule. In order to select the next source, the pool of target sources was examined, and for each source, which was at least 10° above the horizon and which was not previously observed, a score was computed: $S = 100/T_{\rm slew} + 30(20 - \delta) + 0.2E_{\rm min}$, where $T_{\rm slew}$ is the slewing time in seconds, δ is the source declination in degrees, and $E_{\rm min}$ is the minimum elevation of the source among the network stations in degrees. The source from the first group with the maximum score was put in the schedule. If no source from the first group was visible, the source with the highest score from the second group was put in the schedule. Then the procedure was repeated. The slewing rate of VERA stations is 2° s^{-1}, and the acceleration is 2° s^{-2}. The antenna control hardware requires adding a margin of 10 s to the slewing time, and the slewing time should be rounded to the next 4 s. Measurement of system temperature takes an additional 30 s. System temperature was measured either every five scans or when the antennas moved more than 10° from the previous measurement, whichever occurs first. In addition to targets, observations of amplitude calibrator sources were scheduled every hour. At the beginning and end of each session a very strong source, a fringe finder, was observed. The amplitude calibrator sources were taken from the list of 252 sources observed with the K/Q-band survey. The average density of observations was 22 scans per hour.

2.3. *Observations*

GaPS survey observations were scheduled mainly within gaps between regular VERA observations (Table 1). Some observations were performed only at three antennas when one of the stations was not available.

The left-circular polarization in the 21.97–22.47 GHz band was received, sampled with 2 bit quantization, and filtered using the VERA digital filter (Iguchi et al. 2005) before being recorded onto magnetic tapes. The digital filter split the data within the 500 MHz band into 16 frequency channels of 16 MHz width each, equally spaced with spacing 32 MHz. The data were recorded with the SONY DIR2000 recorder at 1 Gbps rate.

3. DATA ANALYSIS

Correlation was carried out on the Mitaka FX correlator (Chikada et al. 1991) with a spectral resolution of 250 kHz. Thus, the amplitude and phase of the cross correlation function at 64 spectral channels within each of the 16 frequency channels was determined. The correlator writes the output in the native CODA format. The output was reformated to the FITS-IDI format (C. Flatter 1998, unpublished).[4] One part of the observing sessions was correlated with accumulation periods of 0.998 s. During the observing campaign it was realized that this accumulation period is too long, and sources with poorly known a priori positions may not be detected. Therefore, the last three experiments were correlated with accumulation periods of 0.1 s. Two experiments, r05343b and r05359d, were recorrelated with accumulation periods of 0.1 s, as well.

The data were analyzed with the program PIMA. The first step of the analysis was fringe fitting. The group delay and delay rate that maximize the fringe amplitude were sought for each baseline independently. The spectrum of the cross-correlation function was presented as a two-dimensional array, with the first dimension running over frequency channels, and the second dimension running over accumulation periods. The size of the matrix was 960×120 for scans with accumulation periods of 1 s, and 1920×1200 for data with accumulation periods of 0.1 s. The grid was extended to 4096×512 and 8192×4096 for the data with 1 and 0.1 s accumulation periods, respectively, with an oversampling factor of 4 by padding extended elements with zeros. The amplitude of the cross-correlation function was normalized by dividing it by the square root of the product of the autocorrelation of the recorded data at each station of the baseline. The two-dimensional fast Fourier transform was performed. The first dimension of the Fourier transform runs over group delays from 0 through 4 mks with steps of 0.49 ns, and the second dimension runs over delay rates from 0 through 4.6×10^{-11} with steps of 0.9×10^{-13} for the data with 1 s accumulation periods, and from 0 through 4.6×10^{-10} with steps of 1.1×10^{-13} for the data with 0.1 s accumulation periods. The coarse search for the maximum of the correlation amplitude was performed over the results of the Fourier transform. In the worst case, when the maximum of the correlation amplitude falls just between the nodes of the grid, the amplitude is reduced by $\mathrm{sinc}^2(\pi/(2v))$, where v is the oversampling factor. When $v = 4$, in the worst case the amplitude is reduced by $16(2 - \sqrt{2})/\pi^2 = 0.95$. The oversampling is important for detecting weak sources. The fine search of the correlation maximum is performed by the consecutive direct Fourier transform at a grid 3×3 around the maximum, reducing the spacings of the grid by half at each step of an iteration. Three iterations of the fine search were performed. Examples of fringe amplitude plots versus trial delay and delay rate for a weak and a strong source are shown in Figures 2 and 3.

One of the experiments, r05349a, was reprocessed with the computer program VEDA, which performs the station-based fringe search using an algorithm similar to that of Alef & Porcas (1986). The results were very close to the results of processing the experiment using the baseline-oriented approach implemented in PIMA. No noticeable gain of the station-based algorithm over the baseline-dependent algorithm was found. Moreover, the station-dependent algorithm failed to detect some sources that the baseline-based algorithm detected only at one baseline because the sensitivity at other stations was poor due to adverse weather conditions. Suppose that there is a station with bad weather in a three-station array. In this case, only one baseline is effective and two baselines that include the affected station may have negative contributions in

[4] Available at http://www.cv.nrao.edu/fits/documents/drafts/idi-format.ps.

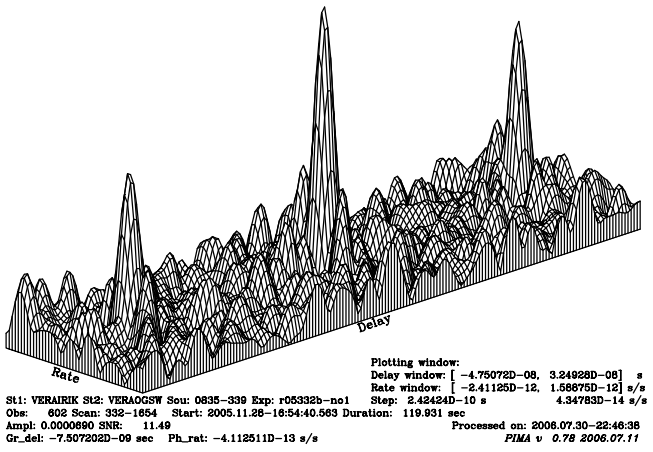

FIG. 2.—Fringe amplitude vs. delay and delay rate for a strong source.

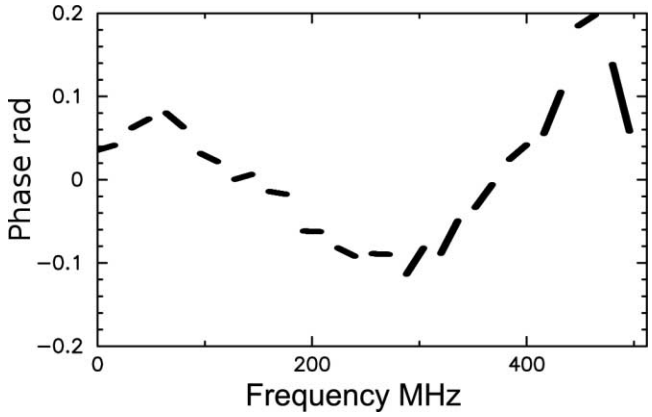

FIG. 4.—Phase of the bandpass calibration at baseline VERAMZSW/VERAOGSW.

finding station based solutions, because data at that baseline just add noise when station-based solutions are searched. We found that the baseline-based algorithm is more suitable for processing these data.

There is another class of station-dependent algorithm, namely, the global fringe search algorithm (Schwab & Cotton 1983). This algorithm potentially may achieve a 40% improvement in source detection at a four-station interferometer Rogers et al. (1995). However, for the global fringe search to work coherently, knowledge of the source structure is very important. If there is a 1 rad phase shift due to the unknown source structure, which is quite likely with VERA baselines, there occurs a coherence loss in the global fringe search and its sensitivity degrades. We did not try this approach, because we do not have enough experience with global fringe search algorithms.

Observations of strong sources with signal-to-noise ratios exceeding 120 were used for evaluation of a baseline-dependent bandpass calibration. The phase of the bandpass calibration was determined as a residual phase with the opposite sign at each spectral channel after subtracting the multiband fringe phase. A linear model was fitted into individual phases at spectral channels within each frequency channel. The amplitude of the bandpass was determined as the ratio of the fringe amplitude at an individual spectral channel to the maximum amplitude within the band. The estimate of the maximum amplitude across the band was found as the maximum value of the amplitude across 1024 spectral channels minus the doubled standard deviation of the amplitude at an individual spectral channel. It was found that the bandpass is stable between experiments, so the bandpasses over all experiments were stacked and averaged. An example of the bandpass calibration is shown in Figures 4 and 5. The complex bandpass calibration was applied to all observations, i.e., the *u-v* data were multiplied with the complex bandpass before the fringe search. This technique increased the fringe amplitude by 5%–15%.

3.1. *Calibration*

System temperatures including atmospheric attenuation were measured with the chopper-wheel method (Ulich & Haas 1976). A microwave absorber at ambient temperature was inserted just in front of the feed horn at the beginning of each scan, and the received total power was measured with a power meter. Using the measured total power for the blank sky and the absorber, we can determine the temperature scale automatically corrected for the atmospheric attenuation. The system temperatures during the best weather conditions were 100–200 K. However, at typical weather conditions $T^{\star}_{\rm sys}$ was 200–500 K, depending on the elevation of observed sources, reaching 2000 K at low elevations and during adverse weather conditions. Figures 6 and 7

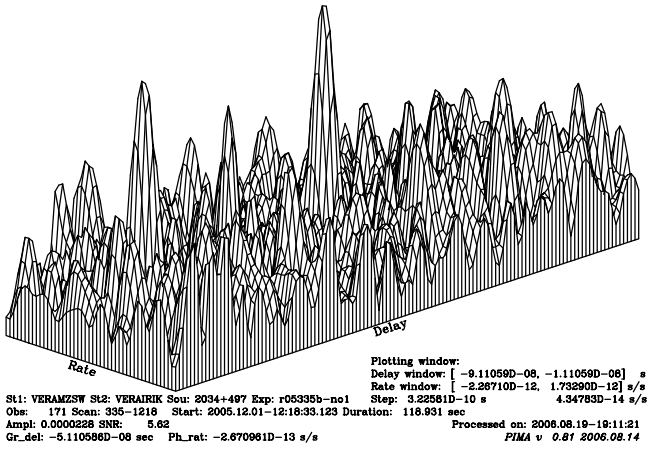

FIG. 3.—Fringe amplitude vs. delay and delay rate for a marginally detected source.

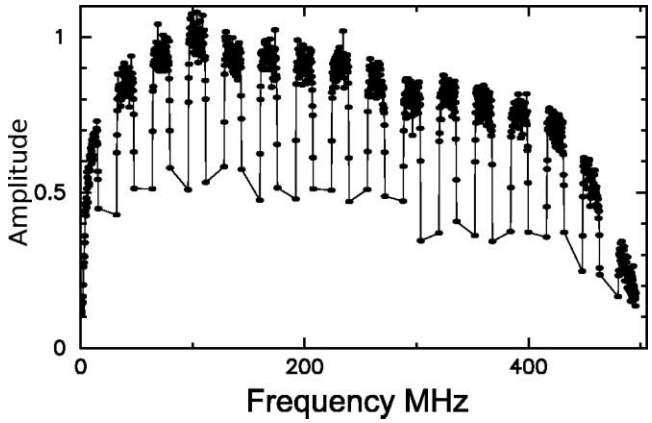

FIG. 5.—Amplitude of the bandpass calibration at baseline VERAMZSW/VERAOGSW.

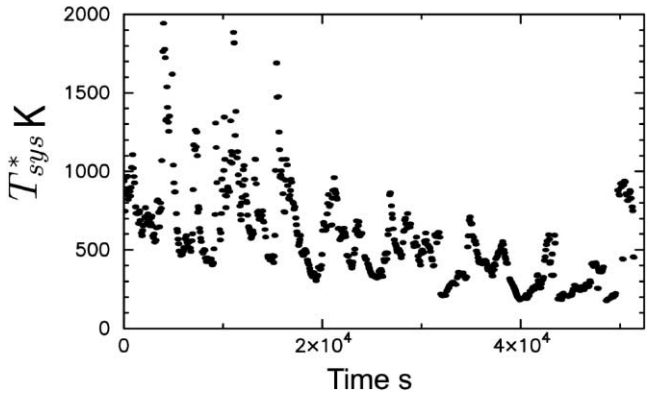

FIG. 6.—System temperature corrected for the atmosphere opacity vs. time from beginning of observing session at VERAISGK on 2005 December 14.

illustrate recorded system temperatures at two stations in good and adverse weather conditions. The uncertainty in the temperature scale was estimated to be 10%, mainly due to the assumption that the ambient temperature is the same as the air temperature.

The aperture efficiency of each antenna was 45%–52% in the 22 GHz band, which was measured by observing the continuum emission from Jupiter once per year. The accuracy of the aperture efficiency measurement was typically 2%–5%. The antenna gain does not show elevation dependency in the elevation range 10°–90°.

Amplitude calibration was performed in two steps. First, the amplitude conversion factor was computed for each observation based on measurements of system temperature and antenna efficiency as $A = (T^\star_{1\mathrm{sys}} T^\star_{2\mathrm{sys}}/g_1 g_2)^{1/2}$, where g_i is the antenna gain. This factor converts dimensionless fringe amplitude to correlated flux density. Then the multiplicative correction to the conversion factor was computed for each observation of the amplitude calibrator at each baseline as $\delta A = F_{\mathrm{kq}}/F_{\mathrm{obs}}$, where F_{kq} is the correlated flux density from maps from the KQ survey and F_{obs} is the observed correlated flux density. The correction δA was averaged over all amplitude calibrators within an individual observing session. The scatter of the individual estimates of the correction provided the measure of errors of amplitude calibration: 20%–25%. Since for the vast majority of sources only 3 or 6 values of fringe amplitude and phase were determined, no attempt to make maps was made.

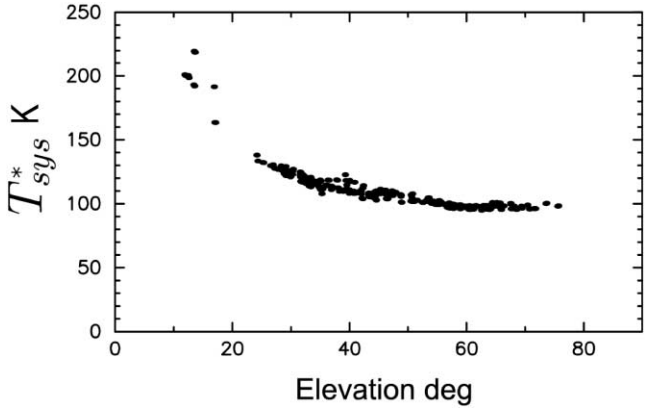

FIG. 7.—System temperature corrected for the atmosphere opacity vs. elevation in degrees at VERAMZSW on 2005 December 9.

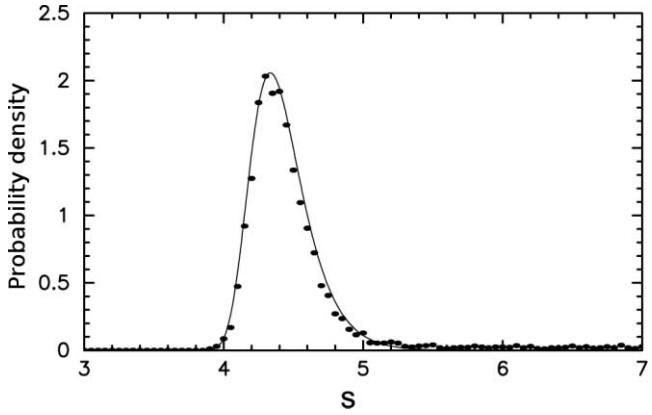

FIG. 8.—Distribution density of the achieved signal-to-noise ratios (*circles*) and the regression curve (*solid line*) $p(s) = (2/\pi)(n_{\mathrm{eff}}/\langle z_{\mathrm{eff}}\rangle)s e^{-s^2/\pi}(1 - e^{-s^2/\pi})^{n_{\mathrm{eff}}-1}$ for scans with accumulation periods of 1.0 s. Here $\langle z_{\mathrm{eff}}\rangle = 1.101$ and $n_{\mathrm{eff}} = 183{,}000$.

3.2. *Detection Limit*

Strong sources have a noticeable peak in plots of fringe amplitude versus trial delay and delay rate, e.g., Figure 2. The presence of noise will force the fringe search process to find a peak in such a plot even in the absence of a signal from the source. For each observation we need to evaluate the probability of false detection. In the absence of signal, the amplitude of the cross-correlation function z has Rayleigh distribution (Papolius 1965):

$$p(z) = \frac{z}{\sigma^2} e^{-(z^2/2\sigma^2)}, \tag{1}$$

where σ is the standard deviation of the real and imaginary part of the cross-correlation function. The noise level of fringe amplitudes was evaluated for each observation. At the grid of cross-correlation function spectrum, 16,384 points were randomly taken and the average amplitude was computed. In order to ensure that no data points with signal were taken, an iterative procedure removed all the points that exceeded the average by more than 4 times. The average amplitude of noise in the spectrum was considered as an estimate of the mathematical expectation of the noise, $\mathcal{E}(z) = (\pi/2)^{1/2}\ \sigma$. In the case in which all points of the spectrum are *statistically independent*, the

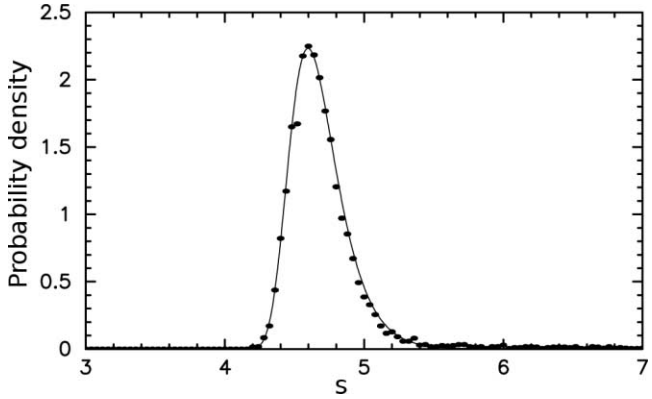

FIG. 9.—Distribution density of the achieved signal-to-noise ratios (*circles*) and the regression curve (*solid line*) $p(s) = (2/\pi)(n_{\mathrm{eff}}/\langle z_{\mathrm{eff}}\rangle)s e^{-s^2/\pi}(1 - e^{-s^2/\pi})^{n_{\mathrm{eff}}-1}$ for scans with accumulation periods of 0.1 s. Here $\langle z_{\mathrm{eff}}\rangle = 1.091$ and $n_{\mathrm{eff}} = 989{,}000$.

TABLE 2
List of Detected Continuum Spectrum Sources

J2000.0 Name (1)	B1950.0 Name (2)	α (J2000.0) (3)	δ (J2000.0) (4)	Detection Status (5)	Correlated Flux Density (Jy) [0, 70] (6)	[70, 100] (7)	[100, 200] (8)	Probability of False Detection (9)	Flag (10)
J0001+6051	2358+605	00 01 07.09	+60 51 22.8	D	...	0.16	0.21	0.0	KNO
J0005+5428	0002+541	00 05 04.36	+54 28 24.9	D	...	0.32	0.28	0.0	KNO
J0006+5050	0003+505	00 06 08.29	+50 50 03.4	D	...	...	0.17	0.0	NEW
J0014+6117	0012+610	00 14 48.79	+61 17 43.5	D	0.29	0.25	0.33	0.0	KNO
J0019+2021	0017+200	00 19 37.85	+20 21 45.6	D	...	0.89	0.91	0.0	KNO
J0019+7327	0016+731	00 19 45.78	+73 27 30.0	D	1.24	1.35	1.28	0.0	KNO
J0021−1910	0018−194	00 21 09.37	−19 10 21.3	M	0.53	0.09	...	5E−03	NEW
J0027+5958	0024+597	00 27 03.28	+59 58 52.9	D	0.35	0.49	0.28	0.0	KNO
J0037−2145	0034−220	00 37 14.79	−21 45 24.5	D	...	0.33	0.12	5E−06	NEW

Notes.— Table 2 is published in its entirety in the electronic edition of the *Astronomical Journal*. A portion is shown here for guidance regarding its form and content. Units of right ascension are hours, minutes, and seconds, and units of declination are degrees, arcminutes, and arcseconds. Source coordinates are taken from the NVSS catalog (Condon et al. 1998). Col. (5): Detection status: D, reliably detected; M, marginally detected. Cols. (6)–(8): Correlated flux density in janskys at three ranges of baseline projections: [0, 70], [70, 100], and [100, 200] megawavelengths. Col. (9): Probability of false detection if it exceeds 10^{-5}, or zero if it is less than 10^{-5}. Col. (10): Flag denoting whether the source was previously detected in the X/S surveys (KNO) or not (NEW).

cumulative probability for the maximum of n points is (Thompson et al. 2001)

$$P(z) = \left[1 - e^{-(z^2/2\sigma^2)}\right]^n. \quad (2)$$

Then, differentiating this expression, we find the probability distribution density of the ratio of the maximal fringe amplitude to the averaged noise at points in the spectrum with no signal, $s = z_{\max}/\langle z\rangle$:

$$p(s) = \frac{2}{\pi}\frac{n}{\langle z\rangle} s e^{-s^2/\pi}\left(1 - e^{-s^2/\pi}\right)^{n-1}. \quad (3)$$

It should be emphasized that expression (3) is valid if all points of the spectrum are independent. This a priori distribution density is an approximation, which is valid only partially due to oversampling and deviation of the bandpass from a rectangular shape. Using the sample of achieved signal-to-noise ratios, we computed the a posteriori distribution density. We assumed that the a posteriori distribution can be approximated as a function like expression (3) with effective parameters $\langle z\rangle_{\rm eff}$ and $n_{\rm eff}$. We found parameters of the distribution that minimize residuals between the a priori and a posteriori distribution densities in the range of signal-to-noise ratios [3, 6.5] by searching through the space of trial values using the brute force algorithm. Plots of the a posteriori maximum of the signal-to-noise ratios and its approximation for the case of accumulation period lengths of 1 and 0.1 s are presented in Figures 8 and 9.

Using effective parameters of the a priori distribution, we can compute the probability that a given observation with the signal-to-noise ratio s belongs to the population of observations without signal from a source as

$$N(s) = 1 - \int_0^s p(s)ds = 1 - \frac{1}{\langle z_{\rm eff}\rangle}\left(1 - e^{-s^2/\pi}\right)^{n_{\rm eff}}. \quad (4)$$

Examining plots of the a posteriori distribution density, we conclude that at the range of signal-to-noise ratios [3.5, 6.5] the share of points that belongs to detected sources is insignificant. Neglecting the population of observations with detected sources slightly inflates our estimates of the probability that an observation belongs to the population of data without signal and makes our estimates of the probability of detection a bit more conservative.

TABLE 3
List of Undetected Sources

J2000.0 Name (1)	B1950.0 Name (2)	α (J2000.0) (3)	δ (J2000.0) (4)	Correlated Flux Density (Jy) Minimum (5)	Average (6)	Maximal Upper Limit (7)	No. Observations (8)	Flag (9)
J0000+3252	2358+326	00 00 49.72	+32 52 56.5	0.11	0.15	0.18	3	NEW
J0000+5539	2357+553	00 00 20.45	+55 39 08.6	0.13	0.15	0.16	3	NEW
J0001+6443	2358+644	00 01 14.95	+64 43 01.1	0.20	0.33	0.88	9	NEW
J0002+5510	2359+548	00 02 00.47	+55 10 38.0	0.15	0.15	0.16	2	NEW

Notes.— Table 3 is published in its entirety in the electronic edition of the *Astronomical Journal*. A portion is shown here for guidance regarding its form and content. Units of right ascension are hours, minutes, and seconds, and units of declination are degrees, arcminutes, and arcseconds. Cols. (5)–(7): Minimum, average, and maximal upper limit of the correlated flux density. These quantities are computed on the basis of the calibrated gain of the interferometer considering what correlated flux density would provide a signal-to-noise ratio of 6.0. Col. (8): Number of observations used in the analysis. Col. (9): Flag denoting whether the source was previously detected at the X/S survey (KNO) or not (NEW).

TABLE 4
Statistics of Observed Sources

Category	Detected	Not Detected
New, continuum spectrum	180	1721
Known, water masers	16	...
Known X/S, continuum spectrum	353	224
Known X/S/K, amplitude calibrators	73	3
Total	549	1945

Each source was observed m times, m typically being in the range 3–6. At a given series of signal-to-noise ratios, a source has k observations with signal-to-noise ratio greater than $s_{\rm lim}$. The probability of false detection $p_{\rm lim}$ corresponds to it. Then for a case in which $p_{\rm lim}$ is so small that we can neglect terms of $p_{\rm lim}^2$, the probability that this may happen due only to the noise in the data, i.e., a source was not detected in neither of k observations, is

$$N_k = C_m^k \prod_{i=1}^{i=k} N(s_i). \quad (5)$$

We used this expression in order to compute the probability of false detection for each source. The value $p_{\rm lim} = 0.05$ was used for computations.

4. RESULTS AND DISCUSSION

We split the list of 2494 sources into three groups: not detected if the probability of false detection is higher than 10^{-2}; marginally detected if the probability of false detection is in the range $[10^{-5}, 10^{-2}]$; and reliably detected if this probability is less than 10^{-5}.

Careful analysis revealed that 16 detected sources are known water masers. The H_2O line was within the recorded bandwidth. We made a trial fringe search using only one frequency channel, which included the water maser line. The fringe amplitude *decreased* by factor of 4 for continuum sources and *increased* by the same factor for maser sources.

The catalog of 533 detected sources that are not masers is listed in Table 2. Source coordinates are taken from the NRAO VLA Sky Survey (NVSS) catalog (Condon et al. 1998). Column (5) shows the detection status: D, reliably detected; M, marginally detected. The correlated flux density in janskys at three ranges of baseline projections ([0, 70], [70, 100], and [100, 200] megawavelengths) is given in columns (6), (7), and (8). Column (9) gives the probability of false detection if it exceeds 10^{-5}, or zero if it is less than 10^{-5}. Column (10) gives a flag denoting whether the source was previously detected in the X/S surveys (KNO) or not (NEW).

Table 3 lists 1945 nondetected sources. Columns (5), (6), and (7) provide the minimum, average, and maximal upper limit of the correlated flux density. These quantities are computed on the basis of the calibrated gain of the interferometer considering what correlated flux density would provide a signal-to-noise ratio of 6.0. Column (8) gives the number of observations used in the analysis, and column (9) gives a flag denoting whether the source was previously detected at the X/S survey (KNO) or not (NEW).

The statistics of the sample of observed sources are given in Table 4. VERA detected 60% of the known X/S sources and 10% of the new sources. These results are somewhat disappointing. With the best weather conditions, VERA is able to detect sources as weak as 100 mJy with 2 minute integration times. However, even in winter, adverse weather conditions significantly deteriorated the detection limit. We show in Figure 10 the cumulative probability function that a source will have a fringe amplitude signal-to-noise ratio limit greater than 6.0 among 14 observing sessions. This detection limit was computed on the basis of the calibrated gain. This probability distribution characterizes the current averaged VERA single-beam sensitivity in winter when observations are carried out with the integration times of 120 s.

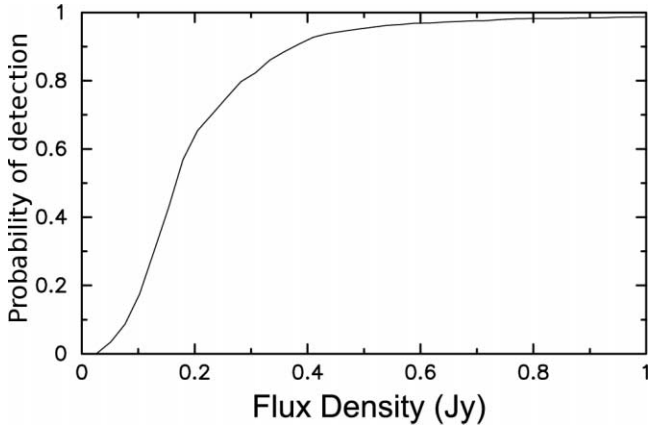

Fig. 10.—Cumulative probability function for a source to have a signal-to-noise ratio above the detection limit 6.0 over 14 observing sessions with VERA at 22 GHz.

Since the 2005f_astro X/S catalog contains 3297 objects within the declination zone $>-40^\circ$, the zone which the VERA can observe, and approximately 60% of the sources from this catalog were detected, we can roughly estimate that the VERA can detect 2000 sources from that list. To date, 252 sources were detected at K band with the VLBA in the K/Q survey, 280 other known X/S calibrators and 180 new sources were detected with the VERA in this campaign, and 64 sources were detected with VERA in various other experiments. In total, the pool of confirmed K-band calibrators is 776 objects.

5. CONCLUDING REMARKS

In the 2005/2006 winter campaign ~2500 sources were observed with VERA during 148 hr. The target sources were either within 6° of the Galactic plane, or within 11° of the Galactic center, or within 2.2° of SiO or H_2O masers. Among them, 533 continuum spectrum and 16 maser sources were detected, including 180 continuum spectrum sources not previously observed with VLBI. The estimates of the correlated flux densities in the ranges [0, 70], [70, 100], and [100, 200] megawavelengths were evaluated. For 1945 nondetected sources the upper limits of their correlated flux densities were evaluated.

The distribution of detected sources over the sky is shown in Figure 11. All detected sources have been observed by the VLBA at 22 GHz in 2006 June–October for imaging and determination of their positions with 1–10 nrad accuracies (L. Petrov et al. 2007, in preparation). Tables of detected and nondetected sources, plots of system temperatures, fringe plots, and other auxiliary information related to this campaign can be found at the Vera Fringe Survey Web site.[5]

[5] See http://vlbi.gsfc.nasa.gov/fss.

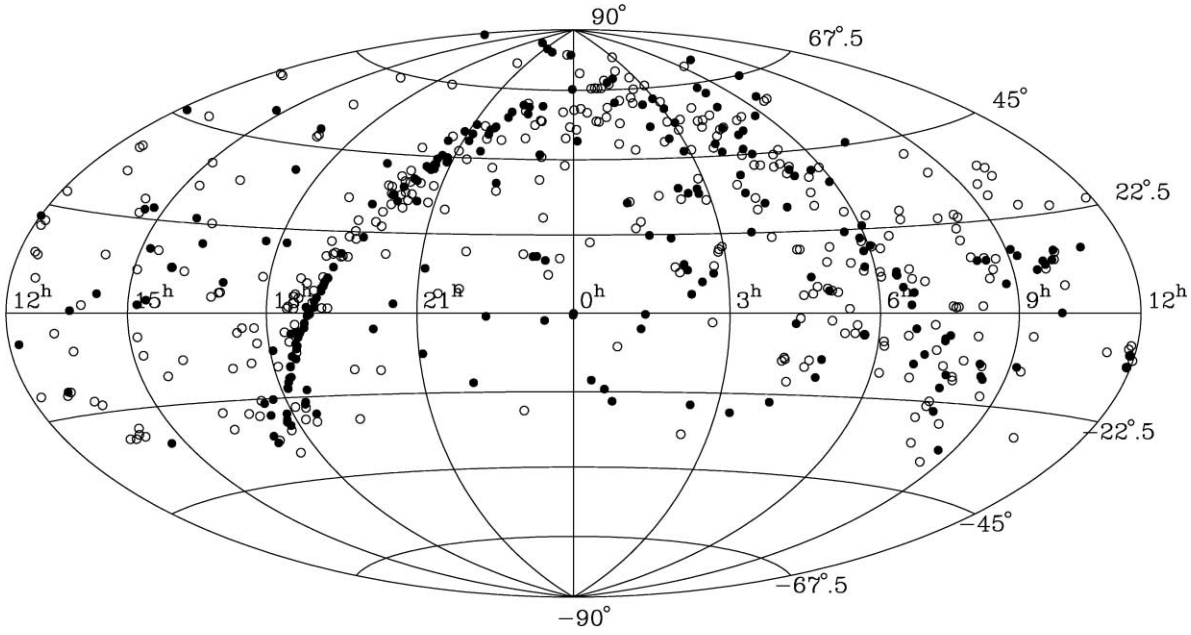

FIG. 11.—Distribution of detected sources over the sky. Filled circles designate new compact sources not observed before with VLBI, and open circles designate known sources observed before at X band with the VLBA. Coordinates are right ascension and declination.

Analysis of the VERA fringe survey data shows that the probability of detecting a 100 mJy source with 120 s of integration time is about 10%; the probability of detecting a 200 mJy source is 60%; and the probability of detecting a 300 mJy source is 80%. Future development of a next-generation water vapor radiometer (N. Kawaguchi 2006, private communication) promises to allow an increase in integration time and, thus, improved VERA sensitivity.

The authors are thankful to D. Gordon for valuable comments. The authors made use of the database CATS (Verkhodanov et al. 1997) of the Special Astrophysical Observatory. This research has made use of the NASA/IPAC Extragalactic Database (NED), which is operated by the Jet Propulsion Laboratory, California Institute of Technology, under contract with the National Aeronautics and Space Administration.

REFERENCES

Alef, W., & Porcas, R. W. 1986, A&A, 168, 365
Beasley, A. J., Gordon, D., Peck, A. B., Petrov, L., MacMillan, D. S., Fomalont, E. B., & Ma, C. 2002, ApJS, 141, 13
Benson, P. J., Little-Marenin, I. R., Attridge, J., Blais, K., Randolph, D., Woods, T., Rubiera, M., & Keefe, H. 1990, ApJS, 74, 911
Chikada, Y., et al. 1991, in Frontiers of VLBI, ed. H. Hirabayashi, M. Inoue, & H. Kobayashi (Tokyo: Universal Acad. Press), 79
Cohen, M. H., & Shaffer, D. B. 1971, AJ, 76, 91
Condon, J. J., Cotton, W. D., Greisen, E. W., Yin, Q. F., Perley, R. A., Taylor, G. B., & Broderick, J. J. 1998, AJ, 115, 1693
Fey, A., Boboltz, D. A., Charlot, P., Fomalont, E. B., Lanyi, G. E., & Zhang, L. D. 2005, in ASP Conf. Ser. 340, Future Directions in High-Resolution Astronomy, ed. J. Romney & M. Reid (San Francisco: ASP), 514
Fomalont, E., Petrov, L., McMillan, D. S., Gordon, D., & Ma, C. 2003, AJ, 126, 2562
Honma, M., Kawaguchi, N., & Sasao, T. 2000a, Proc. SPIE, 4015, 624
Honma, M., et al. 2000b, PASJ, 52, 631
———. 2003, PASJ, 55, L57
Iguchi, S., Kurayama, T., Kawaguchi, N., & Kawakami, K. 2005, PASJ, 57, 259
Jacobs, C. S., Lanyi, G. E., Naudet, C. J., Sovers, O. J., & Zhang, L. D. 2005, in ASP Conf. Ser. 340, Future Directions in High-Resolution Astronomy, ed. J. Romney & M. Reid (San Francisco: ASP), 523
Kawaguchi, N., Sasao, T., & Manabe, S. 2000, Proc. SPIE, 4015, 544
Kobayashi, H., et al. 2004, in Developments in VLBI Science and Technology, ed. R. Bachiller et al. (Toledo: Obs. Astron. Nac. Spain), 275
Kovalev, Y. Y., Petrov, L., Fomalont, E. B., & Gordon, D. 2007, AJ, 133, 1236
Ma, C., et al. 1998, AJ, 116, 516
Papolius, A. 1965, Probability, Random Variables, and Stochastic Processes (New York: McGraw)
Petrov, L., Kovalev, Y. Y., Fomalont, E., & Gordon, D. 2005, AJ, 129, 1163
———. 2006, AJ, 131, 1872
Rogers, A. E. E., Doeleman, S. S., & Moran, J. M. 1995, AJ, 109, 1391
Schwab, F. R., & Cotton, W. D. 1983, AJ, 88, 688
Thompson, A. R., Moran, J. M., & Swenson, G. W. 2001, Interferometry and Synthesis in Radio Astronomy (New York: Wiley)
Ulich, B. L., & Haas, R. W. 1976, ApJS, 30, 247
Valdettaro, R., et al. 2001, A&A, 368, 845
Verkhodanov, O. V., Trushkin, S. A., Andernach, H., & Chernenkov, V. N. 1997, in ASP Conf. Ser. 125, Astronomical Data Analysis Software and Systems VI, ed. G. Hunt & H. E. Payne (San Francisco: ASP), 322
Wrobel, J. M., Patnaik, A. R., Browne, I. W. A., & Wilkinson, P. N. 1998, BAAS, 30, 1308